Nanostructure Assembly

DOI: 10.1002/anie.201406331

Recrystallization-Induced Self-Assembly for the Growth of Cu_2O Superstructures**

Yang Shang, Yi-Ming Shao, Dong-Feng Zhang, and Lin Guo**

Abstract: *The assembly of inorganic nanoparticles (NPs) into 3D superstructures with defined morphologies is of particular interest. A novel strategy that is based on recrystallization-induced self-assembly (RISA) for the construction of 3D Cu_2O superstructures and employs Cu_2O mesoporous spheres with diameters of approximately 300 nm as the building blocks has now been developed. Balancing the hydrolysis and recrystallization rates of the CuCl precursors through precisely adjusting the experimental parameters was key to success. Furthermore, the geometry of the superstructures can be tuned to obtain either cubes or tetrahedra and was shown to be dependent on the growth behavior of bulk CuCl. The overall strategy extends the applicability of recrystallization-based processes for the guided construction of assemblies and offers unique insights for assembling larger particles into complicated 3D superstructures.*

Over the past decades, the research focus of nanoscience and nanotechnology has gradually moved from the controlled preparation of individual inorganic nanoparticles (NPs) to their self-assembly into superstructures,[1] which is promoted by their bulk properties (e.g., plastic metals[2]) and possible new collective physiochemical properties.[3] To date, self-assembly was mainly employed for the construction of ordered two-dimensional (2D) or three-dimensional (3D) superlattices[3,4] and colloidal crystals.[5] The assembly of inorganic NPs into complex 3D superstructures, even with defined morphologies, is still at a preliminary stage.

The assembly of inorganic NPs into 3D superstructures with defined morphologies is of particular interest. It may form the basis of a new engineering strategy where simple and elegant manufacturing methods replace the mechanical assembly of individual parts.[6] Unfortunately, successful cases are limited in this aspect. The implicated strategies of the few impressive demonstrations involve the encoding of binary mixtures of nanoparticles to mimic the atomic/ionic crystallization by achieving a precise balance among intricate interactions.[7] Furthermore, two factors have prevented their wide application: the limited building block sizes (commonly less than 10 nm), which are due to the limited length scale of the molecular forces within the colloidal interface, and the inevitable insulating organic barriers among the subunits. It is thus desirable to explore new routes and driving forces to guide the construction of 3D superstructures.

Aggregation-based processes, with oriented attachment as a special case, have been shown to be one of the important mechanisms that govern the crystal growth in the nano- or sub-micrometer regime.[8] Subunits with dimensions on the millimeter scale as reported very recently[8b] can be jointed together spontaneously, which reveals that "crystal recognition" is a rather strong force. However, thus far, studies of this process have been restricted to the investigation of the growth process itself. How this process could be applied for the guided construction of 3D superstructures has not been addressed. Herein, we explore a novel strategy for the controlled formation of 3D assemblies by taking advantage of an aggregation-based re-crystallization process. This is the first time that the concept of recrystallization-induced self-assembly (RISA) has been applied. Cu_2O 3D superstructures with defined geometries (including cube-like and tetrahedron-like structures) were successfully constructed using Cu_2O mesoporous spheres (MPS) with diameters of approximately 300 nm as the building blocks.

The key of this unique strategy lies in kinetically manipulating the balance between the hydrolysis and recrystallization rates of freshly prepared CuCl precursors (Supporting Information, Figure S1). It is known that CuCl would hydrolyze when dispersed in an aqueous solution with pH values greater than 5.0 according to a two-step reaction process as shown below:[9]

$$CuCl + H_2O \rightleftharpoons CuOH + Cl^- + H^+ \quad (1)$$

$$2\,CuOH = Cu_2O + H_2O \quad (2)$$

As the decomposition of CuOH is a fast process owing to its thermodynamic instability, the rate-determining step of the whole process is the hydrolysis of CuCl into CuOH [Eq. (1)]. Obviously, the process shown in Equation (1) is reversible, and the reaction direction can be influenced by the concentration of the H^+ and/or Cl^- ions, which can be elaborated quantitatively by the standard hydrolysis equilibrium constant $K^{\circ}_{Eq(1)}$:

$$K^{\circ}_{Eq(1)} = [H^+][Cl^-] = \frac{K^{\circ}_w[Cl^-]}{[OH^-]} = \frac{K^{\circ}_w[Cu^+][Cl^-]}{[Cu^+][OH^-]} = \frac{K^{\circ}_w K^{\circ}_{sp}(CuCl)}{K^{\circ}_{sp}(CuOH)} = 1.72 \times 10^{-7} \quad (3)$$

[*] Y. Shang, Y. Shao, Prof. Dr. D. F. Zhang, Prof. Dr. L. Guo
School of Chemistry and Environment, Beihang University
Beijing 100191 (P.R. China)
E-mail: dfzhang@buaa.edu.cn
guolin@buaa.edu.cn

[**] This project is supported by the National Key Basic Research Program of China (2010CB934700), the National Natural Science Foundation of China (21173015 and 51272012), and the Innovation Foundation of BUAA for PhD Graduates.

Supporting information for this article is available on the WWW under http://dx.doi.org/10.1002/anie.201406331.

$K_w^\ominus$ is the ion product constant of H_2O, and $K_{sp}^\ominus(CuCl)$ and $K_{sp}^\ominus(CuOH)$ are the solubility products of CuCl and CuOH, respectively ($K_w^\ominus = 1\times10^{-14}$, $K_{sp}^\ominus(CuCl) = 1.72\times10^{-7}$, $K_{sp}^\ominus(CuOH) = 1\times10^{-14}$).[10] The H^+ and Cl^- concentrations are given by $[H^+]$ and $[Cl^-]$, respectively.

According to the chemical reaction isotherm ($\Delta_r G_m = -RT\ln K^\ominus + RT\ln Q$, where $\Delta_r G_m$ is the Gibbs free energy change, $K^\ominus$ is the standard equilibrium constant, Q is the reaction quotient, R is the universal gas constant, and T is the reaction temperature), the reaction will move in the forward direction when $Q < K^\ominus$, whereas it will move in the reverse direction when $Q > K^\ominus$. When Q is equal to $K^\ominus$, the reaction will reach equilibrium. Considering the prospect of the crystallization, the hydrolysis process [forward reaction in Eq. (1)] would lead to the disintegration of the CuCl crystals, whereas the regeneration process [reverse reaction in Eq. (1)] would facilitate its recrystallization. What would happen during such conflicting processes? To answer this question, we performed a series of experiments by precisely adjusting $[H^+]$ and/or $[Cl^-]$ while keeping other parameters identical to change the degree of hydrolysis against recrystallization, and we defined $\xi = Q/K^\ominus$. Scanning electron microscopy (SEM) images (Figure 1) clearly summarize the relationship between

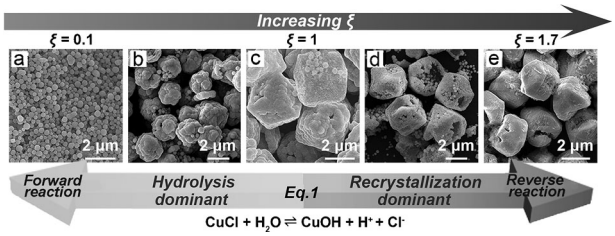

Figure 1. The morphologies and compositions of the products depend on the ratio of the reaction quotient Q to the standard equilibrium constant $K^\ominus$ ($\xi = Q/K^\ominus$). a) Monodisperse Cu_2O spheres. b) Irregular assembly of Cu_2O spheres. c) Cube-like assembly of Cu_2O. d) Cu_2O loose assembly. e) CuCl polyhedra.

ξ and the morphology of the final products, and the corresponding X-ray diffraction (XRD) patterns verified their phase structures (Figure S2). When ξ was very small ($\xi \approx 0.1$), the hydrolysis process dominated. After 45 minutes of reaction, monodisperse Cu_2O MPS formed, as we have previously described (Figure 1a; see also Figures S2a and S3).[11] In contrast, when ξ was quite large ($\xi > 1.7$), the hydrolysis process was almost entirely suppressed. Even when the reaction was run for four hours, the product solely consisted of irregular CuCl polyhedrons (Figure 1e; see also Figure S2e). Remarkably, cube-like Cu_2O superstructures formed when ξ was approaching one (Figure 1c; see also Figure S2c), and the hydrolysis rate approached the recrystallization rate. On a slight deviation from the balance, that is, when the recrystallization rate was slower ($1 > \xi > 0.1$) or faster ($1.7 > \xi > 1$) than the hydrolysis rate, the Cu_2O assemblies would become imperfect (Figure 1b,d; see also Figure S2b, d).

A broad-view SEM image (Figure 2a) indicates the high yield and the quite uniform sizes of the ensembles (ca. 3 μm).

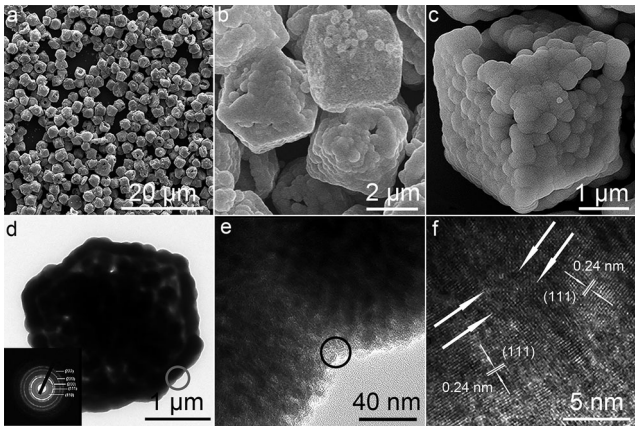

Figure 2. a–c) SEM images of the Cu_2O cube-like superstructures with different magnifications. d) TEM image of a typical Cu_2O superstructure. The inset shows the corresponding SAED patterns. e) Magnified TEM image of the circled area in (d). f) HRTEM image of the circled area in (e). The white arrows in (f) indicate the particle boundaries.

XRD characterization (Figure S4a) verified the cubic Cu_2O phase (JCPDS: 05-0667). The novel structure consists of fused neighboring Cu_2O spheres with diameters of approximately 300 nm (Figure 2c), and some loosely assembled Cu_2O spheres could be identified on the surface of some superstructures (Figure 2b). High-magnification transmission electron microscopy (TEM) images (Figure 2e) recorded at the edge of an individual superstructure (Figure 2d) highlight the mesoporous structure of the building blocks. The measured lattice space in the high-resolution (HR) TEM image (Figure 2f) was approximately 0.24 nm, which agrees well with the (111) crystal plane of cubic Cu_2O. The detailed structure features can be seen more clearly in HRTEM images that were recorded on an individual subunit of the superstructure (Figure S5). The selected area electron diffraction (SAED) pattern of the Cu_2O superstructures (Figure 2d, inset) shows discontinuous bright diffraction rings, revealing their polycrystalline nature.

Time-dependent XRD results confirmed that Cu_2O superstructures had evolved from CuCl (Figure S6). In conjunction with the corresponding TEM results (Figure 3 and 4) and energy-dispersive spectroscopy (EDS) data (Figure S7), the whole process can be divided into three stages. During stage 1 (0–50 min), the large CuCl microcrystals gradually disintegrated into CuCl gels with hydrolyzation, which produced CuCl colloidal spheres (CSs) with embedded Cu_2O NPs (Figure 3c). After aging for 10 minutes, some Cu_2O NPs (ca. 6 nm) wrapped in CuCl gels could be identified although the CuCl microstructure still dominated (Figure 3a, see also Figure S6a, S7a). After 30 minutes, the number of large CuCl particles sharply decreased (Figure S8), while the amount of Cu_2O NPs greatly increased (Figure 3b; see also Figure S7b), which tended to aggregate into CSs with diameters of approximately 100 nm. Spherical aggregation is expected to be the preferred form as it lowers the surface energy and thus minimizes the overall energy.[12] Furthermore, the formation of soluble $[CuCl_x]^{1-x}$ particles by the complexation of insoluble CuCl and Cl^- ions might also contribute to the disintegration of CuCl.[13]

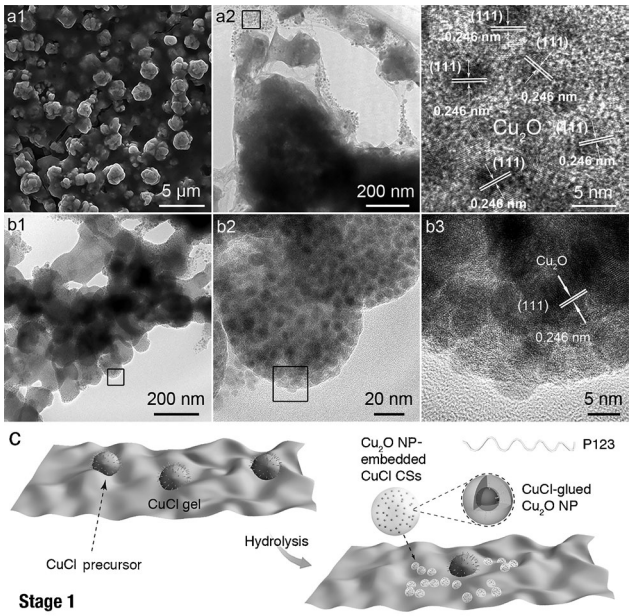

Figure 3. SEM and TEM images of the intermediates obtained after aging for a) 10 and b) 30 minutes. a1) SEM image. a2) TEM image of the gels. a3) HRTEM image of the framed area in (a2). b1) TEM image of CuCl colloidal spheres with embedded Cu_2O NPs. b2) Magnified TEM image of the framed area in (b1). b3) HRTEM image of the framed area in (b2). c) Formation process of the CuCl CSs with embedded Cu_2O NPs (stage 1).

During stage 2 (50–80 min), the CSs formed superstructures in a stepwise assembly process. The CSs first connected into network-like structures (Figure 4a; see also Figure S9), particularly with the formation of some right-angle frames when the reaction proceeded to 50 minutes. After 70 minutes, a large amount of quasi-3D open cages had formed (Figure 4b). Subsequently, the CSs filling generated the rudimentary 3D superstructures with regular shapes (Figure 4c). TEM images (Figure S10a) revealed that a layer of film was adhered to the spherical building blocks, which consisted of large numbers of tiny Cu_2O NPs adhered to CuCl gels. EDS data (Figure S7d) showed that the proportion of the CuCl particles was still quite large, indicating that the hydrolysis of the CuCl particles had not yet reached completion. The absence of diffraction peaks arising from CuCl in the XRD patterns (Figure S6c–S6e) confirmed the amorphous nature of the gel-like structure. At this stage, the Cu_2O NPs within the spherical building blocks still lacked an overall crystallographic orientation (Figure S10b).

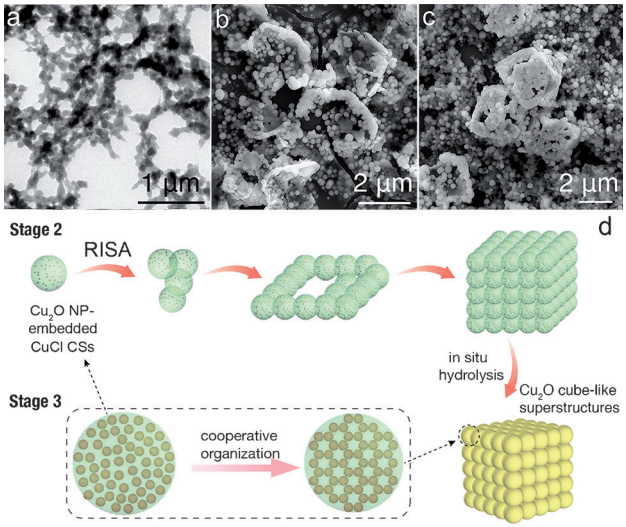

Figure 4. a–c) TEM and SEM images of the intermediates obtained after aging for a) 50, b) 70, and c) 80 minutes. d) Self-assembly process (stage 2) and the in situ hydrolysis and cooperative organization process for the formation of Cu_2O cube-like superstructures (stage 3).

During stage 3 (80–90 min), the ordered mesoporous structure was observed to be in the subunit that formed on depletion of the CuCl particles. With a layer of CuCl covered, the onset of the cooperative organization between the Cu_2O NPs and PEO_{20}–PPO_{70}–PEO_{20} [poly(ethylene oxide)–poly(propylene oxide)–poly(ethylene oxide); P123] is difficult. By continuous in situ hydrolysis, the CuCl was depleted (Figure S7e), and the resulting Cu_2O NPs rotated themselves within the subunits to reach the correct configuration to cooperatively organize themselves into mesoporous structures with the P123 micelles.[11] Finally, Cu_2O 3D superstructures assembled with MPS as the building blocks were constructed (Figure 4d).

Generally, a "presynthesis strategy" was used to assemble the nanocrystals into superstructures[1,5,7] and involved a two-step process in which the pre-synthesized nanocrystals served as building units for further assembly. The one-step construction of the Cu_2O superstructures indicated that nanocrystal synthesis and self-assembly can be coupled together under some specific conditions. A recent report by Tang and co-workers on the growth of CuS nanowire arrays is also an example of such a coupled process.[14]

On the basis of the above analysis, a recrystallization-induced self-assembly (RISA) process was proposed for the growth of the Cu_2O superstructures. The key of this unique strategy lies in kinetically manipulating the balance of the hydrolysis and recrystallization rates of the CuCl precursors. According to the RISA strategy, the differences between the structures that were obtained for different ξ values can be easily understood. When $\xi \approx 0.1$, the hydrolysis process took place promptly, and therefore, the CuCl precursors were quickly transformed into Cu_2O particles, which organized into mesoporous spheres under the assistance of P123.[11] As the recrystallization process was negligible, it lacked the driving force for the assembly of the Cu_2O mesoporous spheres, and thus they maintained their dispersed forms (Figure 1a). For $1 > \xi > 0.1$, although the hydrolysis rate remained relatively high, the recrystallization process cannot be ignored. The recrystallization process induced the organization of CuCl CSs with embedded Cu_2O NPs. However, the CuCl glue had completely transformed into Cu_2O before the particles had sufficient time to reach their equilibrium. The rapid aggregation produced quasi-spherical ensembles to reduce the surface energy (Figure 1b). When $\xi = 1$, the forward reaction rate approached the reverse reaction rate. In this case, the consumption rate of CuCl was nearly identical to its formation rate. The simultaneous hydrolysis and recrystalli-

zation processes ensured sufficient ion exchange, and thus the fusion of adjacent spherical building blocks occurred. Vivid evidence for this process was provided by the formation of the CuCl gel film with embedded Cu_2O NPs among the subunits. For face-centered-cubic (fcc) CuCl, a cubic structure is its equilibrium form. Thus, the superstructures assume cube-like geometry (Figure 1c). For $\xi > 1$, the CuCl formation rate exceeded the consumption rate. In other words, after CuCl had crystallized into its stable form, the hydrolysis was still going on. At the latter stage, there was no CuCl "glue" to bind the formed Cu_2O spheres together, which thus resulted in structure disintegration and imperfect ensembles. Consequently, the spherical building block character was more evident in this case, and many dispersed spheres could be identified (Figure 1d). At $\xi > 1.7$, the hydrolysis process could hardly occur as evidenced by the unchanged white color of the precipitate. Thus, the product remained as pure CuCl even after the reaction time was extended to as long as four hours (Figure 1e).

Interestingly, the superstructures could also be shaped into tetrahedra (Figure 5a6) when the amount of the added P123 was doubled (1.224 g) compared to the amount used for the formation of the cube-like structures, while leaving other conditions unchanged. XRD measurements revealed the structure of the Cu_2O phase (Figure S4b), and their mesoporous building block character, which is similar to that of the cube-shaped particles, was observed by HRTEM (Figure S11) and further confirmed by the N_2 adsorption–desorption isotherms (Figure S12). Under these conditions, the molar P123/CuCl ratio, or χ, was 60. The corresponding transformation from CuCl to Cu_2O required 180 minutes to reach completion, which implies that P123 also played a crucial role during the assembly process.

Without P123, the CuCl particles underwent rapid hydrolysis, and the resulting Cu_2O NPs quickly and randomly aggregated into spherical structures, which subsequently disproportionated into copper(0) within 45 minutes (Figure S13). As the ethylene oxide group (PEO) can bind metal ions to form crown-ether-type structures through ion–dipole interactions,[15] a protective layer of P123 was expected to cover the surface of the CuCl precursors through the coordination of the oxygen atoms in P123 to the copper atoms in the CuCl, which would prevent CuCl from undergoing rapid hydrolysis.[16] The important roles of capping ligands for the stability of inorganic nanocrystals have also been described in other reports.[17]

To gain an in-depth understanding, we performed a series of experiments at different χ values by adjusting the added amount of P123 while keeping other parameters the same (Figure 5a). Obviously, χ was critical to the configuration of the superstructures. When χ was small (< 20), the aggregation was rather irregular (Figure 5a2 and 5a3). The ensembles apparently became regular for greater χ values, with $\chi = 30$ as a threshold value for the cube-like structure (Figure 5a4). With further increases in χ, the tetrahedra become more and more prominent (Figure 5a5). As the products do not longer suffer from disproportionation when $\chi > 5$ as demonstrated in Figure S13, we propose that the hydrolysis rate difference caused by P123 cancelled out. Furthermore, Förster and coworkers have reported that when the polymer-chain surface density is high, the polymer chain would form a dense spherical brush on the surface of the NPs, which provides steric stabilization; when the surface density is decreased, the NPs tend to aggregate owing to the depletion of the polymer chains between adjacent NPs.[18] Therefore, the different configurations should result from the different aggregation rates triggered by the steric stabilization with P123. The relationship between the morphology of the superstructure and χ is illustrated in Figure 5b.

Bulk fcc CuCl structures usually feature tetrahedral or cubic morphology.[19] It is well known that the tetrahedron is the kinetically preferred form as its surface area to volume ratio is much larger than that of the cube,[20] which was also verified in our investigations (Figures S14 and S15). In our case, for higher χ values, the strong steric stabilization would not only retard the hydrolysis of the CuCl precursors but also lower the effective collision among the CuCl CSs with embedded Cu_2O NPs in later stages, and thus the overall recrystallization process will be in kinetically controlled. The Cu_2O superstructure preferentially assumed a tetrahedral structure. In contrast, for relatively low χ values (ca. 30), the steric stabilization was weakened accordingly. The accelerated recrystallization facilitated the formation of the thermodynamically stable form, which is a cube-like structure for bulk CuCl. Thus, it is reasonable to propose that the growth mode of the Cu_2O superstructures resembles the growth behavior of bulk CuCl. Figure S16 clearly substantiates the similarities in shape evolution with the χ value between pure

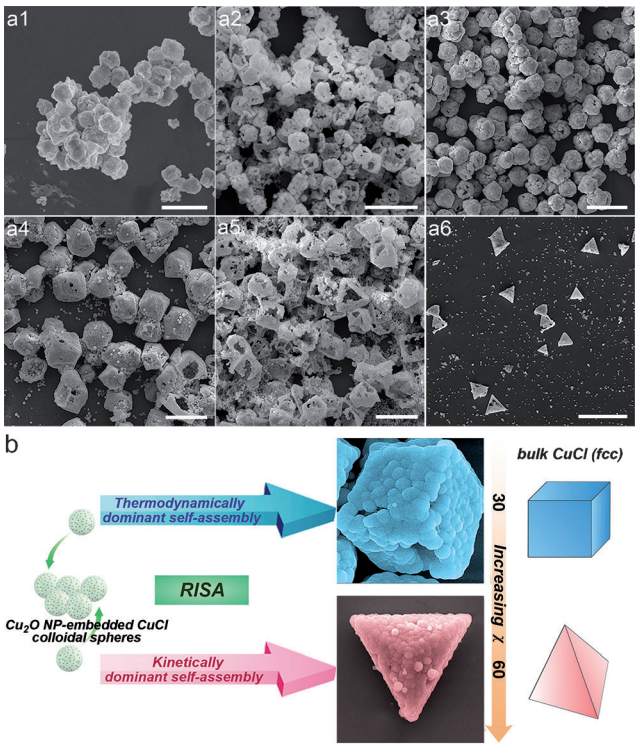

Figure 5. a) SEM images of the products obtained with χ values of a1) 5, a2) 10, a3) 20, a4) 30, a5) 40, and a6) 60, respectively. Scale bar = 5 μm. b) Correlation between the geometry of the Cu_2O superstructures and their self-assembly kinetics.

CuCl and the Cu_2O superstructure, which also provided solid evidence for the crystallization-induced nature of the superstructure assembly.

In summary, it was shown that aggregation-based crystallization can be employed to induce the assembly of 3D superstructures. According to this method, we successfully fabricated Cu_2O 3D superstructures with defined geometries using Cu_2O mesoporous spheres with diameters of 300 nm as the building blocks, which are significantly larger than previously used primary subunits in similar configurations (normally less than 10 nm). The dynamic balance between the hydrolysis and recrystallization rates of the CuCl precursors was crucial for the construction of superstructures with defined shapes. More importantly, the geometry of the products could be tuned to obtain either cubes or tetrahedra, which was shown to be dependent on the growth behavior of bulk CuCl. With a unique mesoporous and assembled structure, the Cu_2O superstructures are expected to be promising materials for surface-enhanced Raman scattering (SERS)[21] or micro gas sensors[22] for single-particle detectors, as they do not suffer from signal inconsistencies from measurement to measurement caused by structure variations. As in the present work, the construction of Cu_2O 3D superstructures was induced by an aggregation-based recrystallization process, the applicability of crystallization-based processes for the guided construction of 3D superstructures with defined geometries is significantly expanded, which may help us to create advanced structures and exploit their properties for building up devices.

Received: June 17, 2014
Revised: July 17, 2014
Published online: August 21, 2014

Keywords: cuprous chloride · cuprous oxide · nanostructures · recrystallization · self-assembly

[1] a) G. M. Whitesides, B. A. Grzybowski, *Science* **2002**, *295*, 2418 – 2421; b) Z. H. Nie, A. Petukhova, E. Kumacheva, *Nat. Nanotechnol.* **2010**, *5*, 15 – 25; c) Y. Gao, Z. Y. Tang, *Small* **2011**, *7*, 2133 – 2146; d) Y. S. Xia, Z. Y. Tang, *Chem. Commun.* **2012**, *48*, 6320 – 6336.

[2] R. Klajn, K. J. M. Bishop, M. Fialkowski, M. Paszewski, C. J. Campbell, T. P. Gray, B. A. Grzybowski, *Science* **2007**, *316*, 261 – 264.

[3] a) M. P. Pileni, *Acc. Chem. Res.* **2007**, *40*, 685 – 693; b) W. Z. Li, L. Kuai, L. Chen, B. Y. Geng, *Sci. Rep.* **2013**, *3*, 2377 – 2381; c) L. Z. Zhou, L. Kuai, W. Z. Li, B. Y. Geng, *ACS Appl. Mater. Interfaces* **2012**, *4*, 6463 – 6467.

[4] E. V. Shevchenko, D. V. Talapin, N. A. Kotov, S. O'Brien, *Nature* **2006**, *439*, 55 – 59.

[5] a) F. Bai, D. S. Wang, Z. Y. Huo, W. Chen, L. P. Liu, X. Liang, C. Chen, X. Wang, Q. Peng, Y. D. Li, *Angew. Chem. Int. Ed.* **2007**, *46*, 6650 – 6653; *Angew. Chem.* **2007**, *119*, 6770 – 6773; b) T. Wang, J. Q. Zhuang, J. Lynch, O. Chen, Z. L. Wang, X. R. Wang, D. LaMontagne, H. M. Wu, Z. W. Wang, Y. C. Cao, *Science* **2012**, *338*, 358 – 363; c) C. Huang, Y. Li, Y. Song, Y. Li, H. Liu, D. Zhu, *Adv. Mater.* **2010**, *22*, 3532 – 3536; d) M. L. Pang, A. J. Cairns, Y. L. Liu, Y. Belmabkhout, H. C. Zeng, M. Eddaoudi, *J. Am. Chem. Soc.* **2013**, *135*, 10234 – 10237; e) X. W. Xu, X. M. Zhang, C. Liu, Y. L. Yang, J. W. Liu, H. P. Cong, C. H. Dong, X. F. Ren, S. H. Yu, *J. Am. Chem. Soc.* **2013**, *135*, 12928 – 12931.

[6] M. Boncheva, G. M. Whitesides, *MRS Bull.* **2005**, *30*, 736 – 742.

[7] a) B. Kowalczyk, K. J. M. Bishop, I. Lagzi, D. W. Wang, Y. H. Wei, S. B. Han, B. A. Grzybowski, *Nat. Mater.* **2012**, *11*, 227 – 232; b) E. Auyeung, T. I. Li, A. J. Senesi, A. L. Schmucker, B. C. Pals, M. O. de La Cruz, C. A. Mirkin, *Nature* **2014**, *505*, 73 – 77; c) K. L. Young, M. R. Jones, J. Zhang, R. J. Macfarlane, R. Esquivel-Sirvent, R. J. Nap, J. S. Wu, G. C. Schatz, B. Lee, C. A. Mirkin, *Proc. Natl. Acad. Sci. USA* **2012**, *109*, 2240 – 2245; d) Y. S. Xia, T. D. Nguyen, M. Yang, B. Lee, A. Santos, P. Podsiadlo, Z. Y. Tang, S. C. Glotzer, N. A. Kotov, *Nat. Nanotechnol.* **2011**, *6*, 580 – 587.

[8] a) J. S. Chen, T. Zhu, C. M. Li, X. W. Lou, *Angew. Chem. Int. Ed.* **2011**, *50*, 650 – 653; *Angew. Chem.* **2011**, *123*, 676 – 679; b) C. Viedma, J. M. McBride, B. Kahr, P. Cintas, *Angew. Chem. Int. Ed.* **2013**, *52*, 10545 – 10548; *Angew. Chem.* **2013**, *125*, 10739 – 10742; c) H. Cölfen, S. Mann, *Angew. Chem. Int. Ed.* **2003**, *42*, 2350 – 2365; *Angew. Chem.* **2003**, *115*, 2452 – 2468.

[9] H. Liu, Y. Zhou, S. A. Kulinich, J. J. Li, L. L. Han, S. Z. Qiao, X. W. Du, *J. Mater. Chem. A* **2013**, *1*, 302 – 307.

[10] J. G. Speight, *Lange's Handbook of Chemistry*, 16edth edMcGraw-Hill, New York, **2005**.

[11] Y. Shang, D. F. Zhang, L. Guo, *J. Mater. Chem.* **2012**, *22*, 856 – 861.

[12] S. Z. Li, X. Huang, H. Li, H. Cai, C. L. Gan, F. Boey, H. Zhang, *Small* **2010**, *6*, 2708 – 2715.

[13] Z. Y. Wang, D. Y. Luan, F. Y. Chiang Boey, X. W. Lou, *J. Am. Chem. Soc.* **2011**, *133*, 4738 – 4741.

[14] Y. S. Xiong, K. Deng, Y. Y. Jia, L. C. He, L. Chang, L. J. Zhi, Z. Y. Tang, *Small* **2014**, *10*, 1523 – 1528.

[15] a) P. D. Yang, D. Y. Zhao, D. I. Margolese, B. F. Chmelka, G. D. Stucky, *Nature* **1998**, *396*, 152 – 155.

[16] Y. Min, M. Akbulut, K. Kristiansen, Y. Golan, J. Israelachvili, *Nat. Mater.* **2008**, *7*, 527 – 538.

[17] a) H. Zhang, M. S. Jin, Y. J. Xiong, B. Lim, Y. N. Xia, *Acc. Chem. Res.* **2013**, *46*, 1783 – 1794; b) J. Wei, H. Wang, Y. H. Deng, Z. K. Sun, L. Shi, B. Tu, M. Luqman, D. Y. Zhao, *J. Am. Chem. Soc.* **2011**, *133*, 20369 – 20377.

[18] M. S. Nikolic, C. Olsson, A. Salcher, A. Kornowski, A. Rank, R. Schubert, A. Frömsdorf, H. Weller, S. Förster, *Angew. Chem. Int. Ed.* **2009**, *48*, 2752 – 2754; *Angew. Chem.* **2009**, *121*, 2790 – 2792.

[19] R. C. Hanson, J. R. Hallberg, C. Schwab, *Appl. Phys. Lett.* **1972**, *21*, 490 – 492.

[20] Y. Wang, S. F. Xie, J. Y. Liu, J. Park, C. Z. Huang, Y. N. Xia, *Nano Lett.* **2013**, *13*, 2276 – 2281.

[21] L. Jiang, T. T. You, P. G. Yin, Y. Shang, D. F. Zhang, L. Guo, S. H. Yang, *Nanoscale* **2013**, *5*, 2784 – 2789.

[22] H. G. Zhang, Q. S. Zhu, Y. Zhang, Y. Wang, L. Zhao, B. Yu, *Adv. Funct. Mater.* **2007**, *17*, 2766 – 2771.

